Eur. Phys. J. B **50**, 11–15 (2006)
DOI: 10.1140/epjb/e2006-00143-8

THE EUROPEAN PHYSICAL JOURNAL B

Fusion reactions in plasmas as probe of the high-momentum tail of particle distributions

M. Coraddu[1,a], M. Lissia[1,b], G. Mezzorani[1,c], and P. Quarati[2,d]

[1] Ist. Naz. Fisica Nucleare (I.N.F.N.) Cagliari, 09042 Monserrato, Italy
and
Dipart. di Fisica dell'Università di Cagliari, 09042 Monserrato, Italy
[2] Dipartimento di Fisica, Politecnico di Torino, C. so Duca degli Abruzzi 24, 10129 Torino, Italy
and
Ist. Naz. Fisica Nucleare (I.N.F.N.) Cagliari, 09042 Monserrato, Italy

Received 29 November 2005 / Received in final form 14 December 2005
Published online 12 April 2006 –

Abstract. In fusion reactions, the Coulomb barrier selects particles from the high-momentum part of the distribution. Therefore, small variations of the high-momentum tail of the velocity distribution can produce strong effects on fusion rates. In plasmas several potential mechanisms exist that can produce deviations from the standard Maxwell-Boltzmann distribution. Quantum broadening of the energy-momentum dispersion relation of the plasma quasi-particles modifies the high-momentum tail and could explain the fusion-rate enhancement observed in low-energy nuclear reaction experiments.

PACS. 05.20.Dd Kinetic theory – 25.60.Pj Fusion reactions – 51.10.+y Kinetic and transport theory of gases – 52.70.Nc Particle measurements

1 Introduction

Many-body collisions broaden the relationship between energy and momentum of quasi-particles: a distribution of momenta, which can have long tails, characterizes a quasi-particle with a given energy. Therefore, the momentum distribution can be very different from the one obtained using a sharp correspondence between energy and momentum [1]. Plasmas are typical environments where this effect can be important.

Fusion processes select high-momentum particles that are able to penetrate the Coulomb barrier and are, therefore, extremely sensitive probes of the distribution tail [2–5].

This broadening of the interacting particle energy-momentum dispersion relation has been proposed recently [6,7] as a possible explanation of the strong enhancement of the observed low-energy rate of the reaction $d(d,p)t$ in deuterated metal target [8–12].

In this paper we study the details of this quantum broadening effect using a simple and effective expression for the distributions. In particular, we determine the region of the distribution responsible of the effect. Our method is applied to the specific case of the enhancement observed in the $d(d,p)t$ reaction rate.

[a] e-mail: massimo.coraddu@ca.infn.it
[b] e-mail: marcello.lissia@ca.infn.it
[c] e-mail: giuseppe.mezzorani@ca.infn.it
[d] e-mail: piero.quarati@polito.it

2 Charged particle distribution in plasma

We consider two species (1 and 2) of interacting charged particles with mass, velocity, momentum, energy and density: $m_{1,2}$, $\mathbf{v}_{1,2}$, $\mathbf{p}_{1,2}$, $E_{1,2}$, $n_{1,2}$. Their fusion reaction rate is $r = (1+\delta_{12})^{-1} n_1 n_2 \langle \sigma v_{rel} \rangle$ where the reaction rate per particle is:

$$\langle \sigma v_{rel} \rangle = \int d^3\mathbf{p}_1 \int d^3\mathbf{p}_1 \, \Phi_1(\mathbf{p}_1) \, \Phi_2(\mathbf{p}_2) \, \sigma v_{rel}; \quad (1)$$

$\Phi_{1,2}(\mathbf{p})$ are the momentum distributions of particles 1 and 2 and $v_{rel} = |\mathbf{v}_1 - \mathbf{v}_2|$ is their relative velocity.

The charged-particle fusion cross section σ is conveniently expressed as

$$\sigma(\epsilon_p) = \frac{S(\epsilon_p)}{E} \exp\left(-\sqrt{\frac{E_G}{\epsilon_p}}\right), \quad (2)$$

where $S(\epsilon_p)$ is the astrophysical factor as function of $\epsilon_p = \frac{1}{2}\mu v_{rel}^2 = \frac{p_{rel}^2}{2\mu}$ with μ the reduced mass and $E_G = 2\mu c^2 (Z_1 Z_2^2 \alpha\pi)^2$ the Gamow energy. Note that the cross section depends on the relative momentum p (to stress

this point we write ϵ_p); only in special cases there is sharp relation between the energy of the particle E and ϵ_p, for instance for free particles $E = \epsilon_p$ is the kinetic energy in the center of mass.

In general we may assume a relation of the form [1]:

$$\delta_\gamma(E,\epsilon_p) = \frac{1}{\pi}\frac{\gamma}{(E-\epsilon_p)^2+\gamma^2}, \tag{3}$$

where the width $\gamma = \hbar\nu_{coll}$ depends on the collision frequency $\nu_{coll} = n\sigma_{coll}v_{coll}$.

Even when the energy distribution is Maxwellian $\propto\exp(E/k_bT)$ (we set the Boltzmann constant $k_b = 1$), the resulting momentum distribution

$$\Phi(\epsilon_p)d\epsilon_p = \frac{4\pi p^2 dp\int_0^\infty dE\,\delta_\gamma(E,\epsilon_p)e^{-E/T}}{4\pi\int_0^\infty p^2dp\int_0^\infty dE\,\delta_\gamma(E,\epsilon_p)e^{-E/T}} \tag{4}$$

can be non-Maxwellian. We consider the case of a Maxwellian energy distribution, which is relevant for the deuteron distribution in metals that is discussed in the next section. A more general Fermi distribution, relevant for high-density environments, yields analogous effects and, in particular, a power-law tail for the momentum distribution.

For the sake of concreteness let us consider a Coulombian collisional cross section, $\sigma_{coll} = e^4/\epsilon_p^2$; the resulting dispersion-relation width is

$$\gamma = \hbar n\frac{e^4}{\epsilon_p^2}\sqrt{\frac{2E}{m}} = \left(\frac{E_S}{\epsilon_p}\right)^2\times\sqrt{\frac{E}{E_S}}\times E_S, \tag{5}$$

where the collisional velocity $v_{coll} = \sqrt{2E/m}$ has been used, n is the density and m the mass of the colliding particles, deuterons in the present case. For convenience we have defined the energy scale

$$\begin{aligned} E_S &= \left(\frac{m_e}{m}\right)^{1/5}\left(\frac{n}{n_0}\right)^{2/5}E_0 \\ &= \left(\frac{m_p}{m}\right)^{1/5}\left(\frac{n}{n_0}\right)^{2/5}3.02649\text{ eV}, \end{aligned} \tag{6}$$

where m_e and m_p are the electron and proton masses, $E_0 = (1/2)\alpha^2 m_e c^2$ is the Rydberg energy, $n_0 = (2a_0)^{-3} = 0.843542\times10^{24}\,\mathrm{cm}^{-3}$ a reference density with a_0 the Bohr radius.

Then the dispersion relation can be written as

$$\delta_\gamma(E,\epsilon_p) = \frac{1}{E_S\pi}\frac{(\epsilon_p/E_S)^2\sqrt{E/E_S}}{(\epsilon_p/E_S)^4(E/E_S-\epsilon_p/E_S)^2+E/E_S}, \tag{7}$$

and the momentum distribution is conveniently expressed in terms of the scaled variable $y = \epsilon_p/(TE_S^5)^{1/6}$:

$$\begin{aligned} \Phi\left(\frac{\epsilon_p}{(TE_S^5)^{1/6}},\frac{T}{E_S}\right)d\epsilon_p &= N\left(\frac{T}{E_S}\right) \\ &\times y^{5/2}dy\int_0^\infty dx\frac{\sqrt{x}e^{-x}}{x+y^4\left(y-x\left(\frac{T}{E_S}\right)^{5/6}\right)^2}, \end{aligned} \tag{8}$$

with the normalization

$$\begin{aligned} N^{-1}\left(\frac{T}{E_S}\right) = \\ \int_0^\infty dyy^{5/2}\int_0^\infty dx\frac{\sqrt{x}e^{-x}}{x+y^4\left(y-x\left(\frac{T}{E_S}\right)^{5/6}\right)^2}. \end{aligned} \tag{9}$$

This distribution should be compared to the Maxwellian one obtained when $\delta_\gamma(E,\epsilon_p) = \delta(E-\epsilon_p)$

$$\Phi_M(\epsilon_p/T)\,d\epsilon_p = dz\frac{2}{\sqrt{\pi}}\sqrt{z}e^{-z} \tag{10}$$

with $z = \epsilon_p/T$.

Using the scaled variable $\epsilon_p/(T^{1/6}E_S^{5/6})$, the distribution depends only on the adimensional parameter T/E_S. Both the distribution $\Phi(\epsilon_p)$ and the thermal mean $\langle\sigma\,v_{rel}\rangle$ can be obtained numerically. We have found an analytical approximation for the important physical regime

$$T \ll E_S \tag{11}$$

that is sufficiently accurate and allows a better analysis. In fact, since contributions to the integral for energies $x > 1$ are exponentially suppressed, equation (11) implies that the limit $T/E_S \to 0$ in equations (8) and (9) is well-defined. In this limit the distribution becomes:

$$\begin{aligned} \Phi_0\left(\frac{\epsilon_p}{(TE_S^5)^{1/6}}\right)d\epsilon_p &\equiv \Phi\left(\frac{\epsilon_p}{(TE_S^5)^{1/6}},0\right)d\epsilon_p \\ &= N_0y^{5/2}dy\int_0^\infty dx\frac{\sqrt{x}e^{-x}}{x+y^6}, \end{aligned} \tag{12}$$

where

$$\begin{aligned} N_0^{-1} &= \int_0^\infty dyy^{5/2}\int_0^\infty dx\frac{\sqrt{x}\,e^{-x}}{y^6+x} \\ &= \frac{\pi\sqrt{2}\Gamma(13/12)}{3(1+\sqrt{3})} = 0.51946. \end{aligned} \tag{13}$$

Under condition (11) the distribution depends on the temperature T and density n only through the single scale parameter $T^{1/6}E_S^{5/6} \sim T^{1/6}n^{1/3}$, which replaces the temperature T of the Maxwell-Boltzmann distribution.

An estimate of corrections to this limiting behavior can be obtained by considering the leading corrections to the normalization integral

$$\begin{aligned} N^{-1}(T/E_S) &= N_0^{-1} + \frac{5\pi\Gamma(23/12)}{9(\sqrt{2}+\sqrt{6})}(T/E_S)^{5/6} \\ &\quad + \mathcal{O}\left((T/E_S)^{5/3}\right) \end{aligned} \tag{14}$$

$$\begin{aligned} &= 0.519457 + 0.437082\,(T/E_S)^{5/6} \\ &\quad + \mathcal{O}\left((T/E_S)^{5/3}\right). \end{aligned} \tag{15}$$

In the limit of small and large ϵ_p the momentum distribution (12) behaves like

$$\lim_{\epsilon_p \to 0} \Phi_0(y)dy = N_0\sqrt{\pi}y^{5/2}dy\left(1 - \sqrt{\pi}y^3 + 2y^6 + \mathcal{O}\left(y^9\right)\right) \tag{16}$$

$$\lim_{\epsilon_p \to \infty} \Phi_0(y)dy = N_0\frac{\sqrt{\pi}dy}{2y^{7/2}}\left(1 - \frac{3}{2y^6} + \frac{15}{4y^{12}} + \mathcal{O}\left(y^{-18}\right)\right). \tag{17}$$

Approximations that retain the leading and next-to-leading asymptotic behaviors of the distribution are

$$\Phi_l(y)dy = N_0\sqrt{\pi}y^{5/2}dy\frac{1}{1+2y^6} \tag{18}$$

$$\Phi_{nl}(y)dy = N_0\sqrt{\pi}y^{5/2}dy\frac{1+y^6}{1+\sqrt{\pi}y^3+5y^6+2y^{12}}. \tag{19}$$

The linear combination of the two approximations that maintains the normalization, $\int_0^\infty dy(c\Phi_l(y) + (1-c)\Phi_{nl}(y)) = \int_0^\infty dy\Phi_0(y)$, reproduces $\Phi_0(y)$ within 2%.

The most important lesson we learn from this analysis is that the quantum broadening due to plasma effects produces a distribution whose typical scale is $(TE_S^5)^{1/6}$ instead of T: these two scales can be very different. For instance, deuterons, $m = 2m_p$, at the density $n = 4.38 \times 10^{23}$ cm^{-3} have the energy scale $E_S \approx 2.03$ eV. Therefore, at temperatures $T_1 = 2.44 \times 10^{-2}$ eV and $T_2 = 0.109$ eV, which fulfil condition (11), the scales of the modified distributions are $E_S^{5/6}T_1^{1/6} = 0.770245$ eV and $E_S^{5/6}T_2^{1/6} = 0.988481$ eV, respectively.

This large shift of the particle distribution towards higher energies is demonstrated in Figure 1, where we show $\Phi_0(\epsilon_p)$ from equation (12) compared to the Maxwell-Boltzmann distribution, equation (10), for the two temperatures T_1 and T_2; the target deuteron density of reference [8] has been used as density n of colliding particles: $n = 4.38 \times 10^{23}$ cm^{-3}.

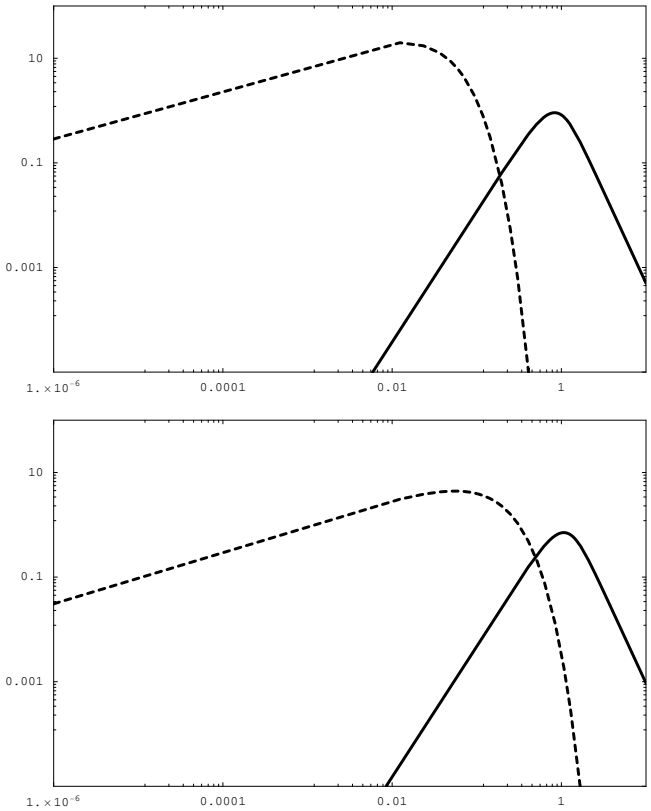

Fig. 1. The momentum distribution function $\Phi_0(\epsilon_p)$ in eV^{-1} (full line) and the Maxwellian one (dashed line) as functions of ϵ_p for two different temperatures $T_1 = 10$ °C $= 0.0244$ eV (upper panel) and $T_2 = 1000$ °C $= 0.109$ eV (lower panel) with density $n = 4.38 \times 10^{23}$ cm^{-3}.

3 The low-energy D(D,P)T reaction rate

The *d(d,p)t* fusion reaction rate has been recently measured using deuterated metal targets in the 4−20 keV energy range [8–12]. At low energy these experiments have found a considerable higher reaction rate than the corresponding one measured using gas targets. Low-energy enhancements are usually explained in terms of electron screening; however, the electron screening potential U_e that would reproduce these measurements in deuterated metals is of the order of hundreds of eV: this potential is much higher than the adiabatic estimate for the maximal screening potential $U_e \leq 28$ eV.

The thermal motion of the target atoms is another mechanism capable of increasing the reaction rate; however, the Maxwellian momentum distribution at the experimental temperatures gives a negligible effects [6,13].

The observation that large enhancements have been observed in deuterated metals but not in insulators [10,12] has suggested a possible explanation based on effects of the plasma of electrons in the metal [11,12]. This simplified model with quasi-free valence electrons predicts an electron screening distance of the order of the Debye length $R_{Deb} = \sqrt{k_bT/(4\pi n_{eff}(Ze)^2)}$, where n_{eff} is the effective density of valence electrons that can be treated as quasi-free. This approach reproduces both the correct size of the screening potential U_e and its dependence on the temperature: $U_e \propto T^{-1/2}$ [10,12].

The problem with this explanation is that the resulting R_{Deb}, for the actual experimental conditions, is about ten times smaller than the Bohr radius a_0; the mean number of quasi-free particles in the Debye sphere N_{Deb}, the so called Debye number [14], is, therefore, much smaller than one: $N_{Deb} = n_{eff}(4\pi/3)R_{\rm Deb}^3 \approx (4\pi/3)n_{eff}(a_0/10)^3 \approx 3 \times 10^{-5}$. The picture of the Debye screening, which should be a cooperative effect with many participating particles ($R_{\rm Deb}$ should be at least greater than the Wigner Seitz radius, which is of the order of the Bohr radius), seems not to be applicable and the observed increase of the *d(d,p)t* reaction rate still missing a consistent explanation. An additional technical inconsistency in the Debye screening explanation [10,12] is the use of a non-degenerate formula for the screening radius in a situation where the electrons are degenerate.

In this context, we apply the analysis presented in the previous section to the discussion of a recent interesting tentative explanation of these puzzling experimental rates, which is based on the quantum-tail effect [6,7].

Since it is a good approximation of the experimental situation to consider the projectile distribution monoenergetic with a sharp relation between energy and momentum $\delta_\gamma(E_{beam},\epsilon_p)=\delta(E_{beam}-\epsilon_p)$, the relative velocity is function only of ϵ_{p_t} and of the angle ϑ between $\mathbf{p}_t$ and the beam: $v_{rel}^2=2(E_{beam}+\epsilon_{p_t}-2\sqrt{E_{beam}\epsilon_{p_t}}\cos\vartheta)/m$. Following the analysis of the previous section, target particles have a Boltzmann-Gibbs energy distribution with a relation between energy and momentum that is broadened by plasma quantum effects and it is given by equation (7). The effective momentum distribution of the target particles is, therefore, not Maxwellian but given by equation (8). Substituting this distribution of target particles, the sharp monoenergetic distribution for projectile particles, and the above relation for the relative velocity in equation (1) the reaction rate per particle becomes

$$\langle\sigma\, v_{rel}\rangle = \int d^3\mathbf{p}_t\, \Phi(\mathbf{p}_t)\,\sigma\, v_{rel} \tag{20}$$

$$= 2\pi m_D^{3/2}\int_{-1}^{+1} d\cos\vartheta \int_0^\infty dE \times \int_0^\infty d\epsilon_{p_t}\sqrt{2\epsilon_{p_t}}\,\delta_\gamma(E,\epsilon_{p_t})\,e^{-E/k_bT} \tag{21}$$

$$= \frac{1}{2}\int_{-1}^{1} d\cos\vartheta \times \int_0^\infty d\epsilon_{p_t}\Phi(\epsilon_{p_t}/(TE_S^5)^{1/6},T/E_S)\sigma\, v_{rel},\sigma\, v_{rel},$$

$$\sigma\, v_{rel} = \frac{4\,S(E_{cm})}{m_D\, v_{rel}}\,\exp\left(-\pi\sqrt{\frac{2E_G}{\mu v_{rel}^2}}\right),$$

where $E_{cm}=\mu v_{rel}^2/2$ and $\mu=m/2$. Since condition $T\ll E_S$ is verified, we can use the simplified form in equation (12)

$$\langle\sigma v_{rel}\rangle = \frac{1}{2}\int_{-1}^{1} d\cos\vartheta\int_0^\infty d\epsilon_{p_t}\Phi_0(\epsilon_{p_t}/(TE_S^5)^{1/6})\sigma\, v_{rel}. \tag{22}$$

As we have analyzed in the previous section, the momentum distribution resulting from the quantum broadening with the chosen collisional cross section has two main features: a peak at energies of the order of $(TE_S^5)^{1/6}$ instead of T and a power-law tail that decreases as $\epsilon_p^{-7/2}$ instead of the exponential cut-off. It is, therefore, physically interesting to separate the contributions from the peak, the high-momentum tail and the low-momentum part of the distribution, so that we can understand which feature(s) of the modified distribution give(s) important corrections to the rate. To this purpose we define the peak of the target momentum distribution as $0.54(TE_S^5)^{1/6}=\epsilon_l<\epsilon_p<\epsilon_h=1.15(TE_S^5)^{1/6}$: this region includes about 50% of the particles and we call the corresponding contribution to the reaction rate per particle $\langle\sigma\, v_{rel}\rangle_C$; the contributions from the low- ($\epsilon_p<\epsilon_l$: about 10% of the particles) and high-momentum ($\epsilon_h<\epsilon_p$: about 40% of the particles) parts are indicated with the subscript L and H.

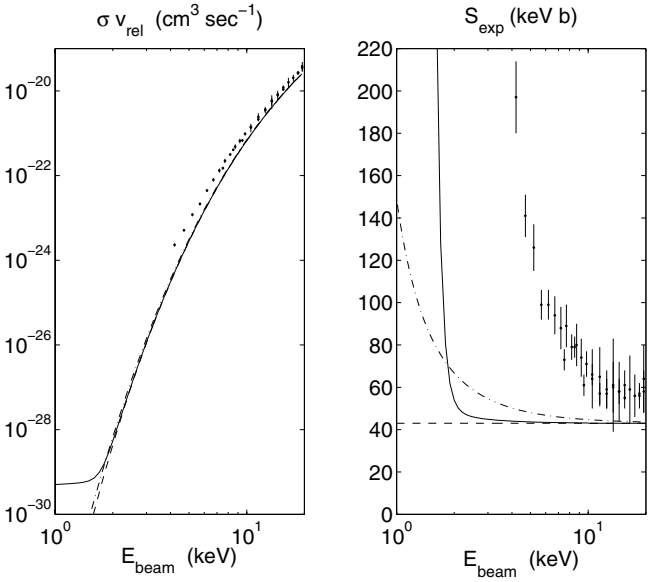

Fig. 2. Reaction rate per particle $(\sigma\, v_{rel})_{T=0}$ (left panel) and the corresponding astrophysical factor $S=(\sigma\, v_{rel})_{T=0}\,\frac{m_D}{4}\sqrt{\frac{2E_{beam}}{m_D}}\exp\left(\pi\sqrt{\frac{2\,E_G}{E_{beam}}}\right)$ (right panel) for the $d(d,p)t$ reaction as function of the beam energy. The experimental data [8] are compared with three theoretical curves: bare nuclei (dashed line), screened nuclei with the adiabatic potential $U_e=28$ eV (dot-dashed line), and our calculation that includes the quantum-tail thermal effect (solid line).

$$\langle\sigma\, v_{rel}\rangle = \langle\sigma\, v_{rel}\rangle_L + \langle\sigma\, v_{rel}\rangle_C + \langle\sigma\, v_{rel}\rangle_H\,. \tag{23}$$

We have used $S(E_{CM})\simeq S_0=43$ keV b (the error is $\leq$6% for $E_{beam}\leq 10$ keV): then the ϑ integral can be done analytically in terms of the incomplete Gamma-Euler function; the remaining integrations have been performed using the Gauss-adaptive method.

The resulting rate is shown in Figure 2 as the thin solid line. In the same figure are shown for comparison the experimental data [8] and the other theoretical curves: the thick solid line shows the rate for bare nuclei, while the dot-dashed line shows the rate with electron screening in the adiabatic limit, which should provide an upper limit to the screening potential, $f_e=\exp\left(\pi\sqrt{\frac{E_G}{E_{cm}}}\,\frac{U_e}{2\,E_{cm}}\right)$.

As it is apparent from Figure 2, the quantum-tail effect is in fact capable to produce a strong enhancement of the reaction rate, but this effect starts only below $E_{beam}\sim 2$ keV; on the contrary the experimental excess starts at energies two or three times higher.

From the analysis of the separate contributions of the three regions (low, central or peak, and high) of the target momentum distribution (see Fig. 3), we observe that the increase of $\langle\sigma\, v_{rel}\rangle$ at low energies ($E_{beam}\sim 2$ keV), shown in Figure 2, is caused mainly by the high momentum particles in the power-law tail, the $\langle\sigma\, v_{rel}\rangle_H$ term: the peak and the low-momentum region seem not contribute to this increment in the present situation.

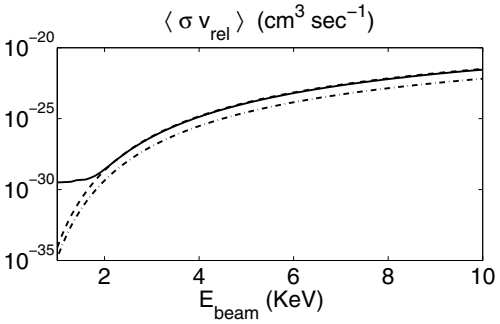

Fig. 3. Contributions to the reaction rate per particle $\langle \sigma\, v_{rel} \rangle$ coming from the three different regions of the target momentum distribution: low-momentum region (dash-dotted line), central or peak region (dashed line), and high-momentum or tail region (solid line).

4 Conclusion

We have studied the effects of the quantum broadening of the relation between energy and momentum due to a specific collisional cross section. An important effect is the considerable modification of the resulting momentum distribution:

(1) the central part of the distribution is shifted from T to $(TE_S^5)^{1/6}$ where the energy scale E_S, equation (6), grows as $n^{2/5}$ with the density n;
(2) the high-momentum tail decreases as a power $\epsilon_p^{-7/2}$ instead of having an exponential cut-off (see Fig. 1).

We have applied this quantum-tail effect to nuclear fusion processes between charged particles at sub-barrier energies of the order of few keV and compared our results with the experimental data relative to the *d(d,p)t* reaction with deuterated target.

Our calculation shows that the quantum-tail effect produces an important increment of the observed reaction rate enhancement at very low energies (∼2 keV). However, this mechanism cannot reproduce the experimental rate for deuterium, which has been found to increase already at higher energies (∼6−8 keV), as shown in Figure 2.

We have also analyzed more in details the effect of the modified momentum distribution on the reaction rate by breaking up the contributions from target particle in three regions: the low-momentum, the central or peak, and the high-momentum region. The strong enhancement of the rate is due essentially to the particles in this last region: the high-momentum power-law tail of the distribution.

We are extending our results by using other collisional cross sections and investigating the temperature dependence of the mechanism.

References

1. V.M. Galitskii, V.V. Yakimets, JEPT **24**, 637 (1967)
2. M. Coraddu, G. Kaniadakis, A. Lavagno, M. Lissia, G. Mezzorani, P. Quarati, Braz. J. Phys. **29**, 153 (1999) [arXiv:nucl-th/9811081]
3. A.N. Starostin, V.I. Savchenko, N.J. Fisch, Phys. Lett. A **274**, 64 (2000)
4. A.N. Starostin, A.B. Mironov, N.L. Aleksandrov, J.N. Fisch, R.M. Kulsrud, Physica A **305**, 287 (2002)
5. M. Lissia, P. Quarati, Europhys. Lett. **36**, 211 (2005) [arXiv:astro-ph/0511430]
6. M. Coraddu, M. Lissia, G. Mezzorani, Y.V. Petrushevich, P. Quarati, A.N. Starostin, Physica A **340**, 490 (2004) [arXiv:nucl-th/0401043]
7. M. Coraddu, G. Mezzorani, Y.V. Petrushevich, P. Quarati, A.N. Starostin, Physica A **340**, 496 (2004) [arXiv:nucl-th/0402025]
8. F. Raiola et al., Eur. Phys. J. A **13**, 377 (2002)
9. F. Raiola et al., Phys. Lett. B **547**, 193 (2002)
10. C. Bonomo et al., Nuc. Phys. A **719**, 37c (2003)
11. F. Raiola et al., Eur. Phys. J. A **19**, 283 (2004)
12. F. Raiola et al., J. Phys. G **31**, 283 (2005)
13. G. Fiorentini, C. Rolfs, F.L. Villante, B. Ricci, Phys. Rev. C **67**, 014603 (2003) [arXiv:astro-ph/0210537]
14. S. Ichimaru, *Statistical plasma physics* (Addison-Wesley, USA, 1992)